Observation of magnetic gradients in stainless steel with a high-Tc superconducting quantum interference device microscope

doi: 10.1063/1.1334637(http://dx.doi.org/10.1063/1.1334637)

Observation of magnetic gradients in stainless steel with a high-T_c superconducting quantum interference device microscope

Yoshimi Watanabe,[a] S. H. Kang, J. W. Chan, and J. W. Morris, Jr.
Center for Advanced Materials, Lawrence Berkeley National Laboratory and Department of Materials Science and Engineering, University of California, Berkeley, California 94720

T. J. Shaw and John Clarke
Department of Physics, University of California, Berkeley and Materials Science Division, Lawrence Berkeley National Laboratory, California 94720

(Received 28 August 2000; accepted for publication 30 October 2000)

Superconducting quantum interference device (SQUID) microscopes may serve as useful nondestructive evaluation (NDE) tools since they can precisely measure the local magnetic field variation that can be related to the characteristics of ferromagnetic materials. To demonstrate this, we have studied magnetic functionally graded materials (FGMs) in the Fe–Cr–Ni alloy system using a high-transition-temperature (HT_c) SQUID microscope. The FGMs were either fabricated by inhomogeneous mechanical deformation or by heat treatment in a temperature gradient. The magnetic properties of these materials were measured using the vibrating sample magnetometer technique along the deformation or the temperature gradients. The results from this technique and the microstructural properties from optical imaging are discussed in conjunction with the magnetic field images obtained from the SQUID microscope. By exploring the results, the feasibility and benefit of utilizing SQUID microscopy as a NDE tool are discussed. © *2001 American Institute of Physics.* [DOI: 10.1063/1.1334637]

I. INTRODUCTION

Superconducting quantum interference devices (SQUIDs) are known as the most sensitive detectors of magnetic flux. The devices can measure any physical quantity that can be converted to a flux, for example, magnetic field, magnetic field gradient, current, voltage, displacement, and magnetic susceptibility.[1] One of its applications is SQUID microscopy. In this work, the samples are first demagnetized and then subsequently magnetized in fields up to 50 mT, and the vertical component of the remanent magnetization is measured by rastering the sample over the SQUID using a two-dimensional (2D) translation stage with a scanning range of 50 mm. The information from the 2D remanent magnetization images may provide an effective method for the nondestructive evaluation (NDE) of magnetic materials through a simple measurement of remanent magnetization.[2]

It is well known that the deformation of the Fe–18Cr–8Ni system (composition in weight percent) induces the formation of the martensite phase α' within its parent austenite phase γ.[3] In addition, this martensitic α' phase can transform into the γ phase (α' to γ reverse martensitic transformation) when the alloy is heated.[4] This reverse martensitic transformation is accompanied by a ferromagnetic (α' phase) to paramagnetic (γ phase) transition. Along the temperature gradient from the starting temperature of the reverse martensitic transformation to the finishing temperature, therefore, the magnitude of the saturation magnetization decreases. This phenomenon has been used to produce a magnetic functionally graded material (FGMs) using an inhomogeneous heat treatment of a deformed 304 stainless steel.[5]

In this study, the magnetic functionally graded materials[6,7] are fabricated either by a inhomogeneous deformation of the wedge-shaped Fe–Cr–Ni alloy or by an inhomogeneous heat treatment of the deformed alloy. The various magnetic properties of these FGMs are measured using the vibrating sample magnetometer (VSM) technique. The magnetic properties are correlated to the microstructures of the materials obtained from optical imaging. These results are then discussed using the magnetic field images generated by the SQUID microscope.

II. SAMPLE PREPARATION

The material used in this study was a commercial grade AISI 304 (Fe–Cr–Ni system) stainless steel bar with a cross section of 12.7 mm×6.4 mm. The chemical composition (wt %) of the stainless steel studied was: Cr 18.46, Ni 9.04, C 0.033, Mn 1.86, Mo 0.28, Co 0.10, Cu 0.41, P 0.028, Si 0.32, S 0.019, Ti <0.005, V 0.05, and Fe bal. From this steel bar, magnetically graded materials were produced by two methods. Samples 1, 2, and 3 were fabricated by rolling a wedge-shaped sample to induce inhomogeneous plastic deformation. Samples A and B were made by heat treating a deformed sample in a thermal gradient.

Wedge-shaped samples were machined from the as-received stainless steel bar, and the dimensions were shown in Fig. 1(a). If the x is taken as shown in Fig. 1(a), and assuming negligible change in the width direction, the distance x_0 becomes x after the rolling:

[a]Permanent address: Department of Functional Machinery and Mechanics, Shinshu University, 3-15-1, Tokida, Ueda 386-8567, Japan; electronic mail: yoshimi@giptc.shinshu-u.ac.jp

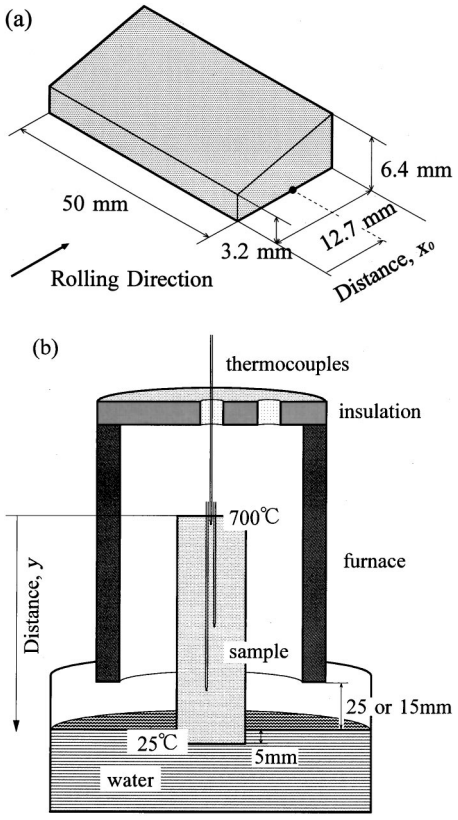

FIG. 1. (a) Schematic illustration of a wedge-shaped sample, in which the thickness of the sample decreases linearly. (b) Schematic illustration of heat treatment conditions resulting in temperature gradient along specimen.

$$x=\left(\frac{3.2x_0}{25.4}+3.2\right)\frac{x_0}{t}, \tag{1}$$

where t is the thickness of the sample after the rolling.[8] Therefore, the rolling ratio at x position, $R(x)$, is

$$R(x)=1-\frac{12.7t}{3.2x_0+40.64}. \tag{2}$$

An extensive description of the fabrication method of Samples 1, 2, and 3 is presented elsewhere.[8]

Figure 1(b) is a schematic illustration of the inhomogeneous heat treatment. After austenitization at 1323 K (1050 °C) for 2 h, the samples were rolled down to a rolling ratio of 70% to introduce the initial α' martensite phase. X-ray diffraction patterns of the samples showed a mixture of austenite and martensite phases. Each sample was then heated in a furnace while one end of the sample was immersed in water. As a result, a temperature gradient was developed along the sample. The temperature gradient was controlled by changing the gap between the furnace and water: 25 and 15 mm for samples A and B, respectively. During the heat treatment, the temperatures at different locations were measured by the thermocouples attached to the sample. Figure 2 shows the temperature gradients during the heat treatment. In this figure, distance, y, indicates the sample positions, i.e., distances from the top of the sample, as shown in Fig. 1(b). It is known that the starting and finishing temperatures of the reverse martensitic transformation are 450° and 650 °C, respectively. Therefore, the magnetic properties of the samples are expected to change over the region from $y=15$ mm to $y=45$ mm for sample A and from $y=20$ mm to $y=50$ mm for sample B. This reverse transformation is completed very quickly. For example, more than 80% of the reverse transformation occurs within 15 min when the sample is heated at 670 °C.[4] The holding time was, therefore, set at 15 min, and the samples were then immediately quenched in water.

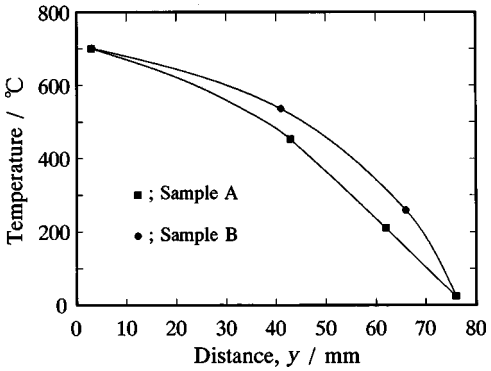

FIG. 2. Temperature gradients during the thermal gradient heat treatment.

Both the rolled (samples 1, 2, and 3) and the heat-treated samples (samples A and B) were cut into two pieces by an electrodischarge machine. One piece was mounted in Transoptic™ powder for the SQUID microscope and optical imaging. Since the penetration depth of the SQUID microscope is large while the thickness of the samples was relatively thin, there is a possibility that the SQUID image includes the information from the opposite surface. Therefore, both surfaces were polished carefully before the mounting. The other piece was cut by an electrodischarge machine into smaller pieces (1 mm in width) along the direction perpendicular to the gradient for the VSM measurements.

III. MEASUREMENT AND SQUID MICROSCOPE

Magnetic measurements were made in a vibrating sample magnetometer (VSM) to obtain quantitative magnetic-property profiles in the samples. The hysteresis curve of each piece was then generated at room temperature with a maximum magnetic field of 1.2 MA/m. The saturation magnetization and remanent magnetization were evaluated from the hysteresis curves. Since the magnetic field was applied along the longitudinal direction of the samples, the influence of demagnetization on the hysteresis curve was assumed negligible. The magnetic properties were correlated to the optical microstructures of the materials. A magnetic etching technique was used to reveal the ferromagnetic α' martensite phase within the paramagnetic austenite phase.[9]

The SQUID microscope used in this study is similar in design to other SQUID microscopes,[10] with the additional advantage of having a rather large (50 mm×50 mm) scanning range. It consists of a SQUID inside a vacuum enclosure that is thermally coupled to a liquid nitrogen reservoir, as shown schematically in Fig. 3, with a 125-μm-thick sapphire window separating the SQUID from room temperature and pressure. A sample stage with three height-adjustment

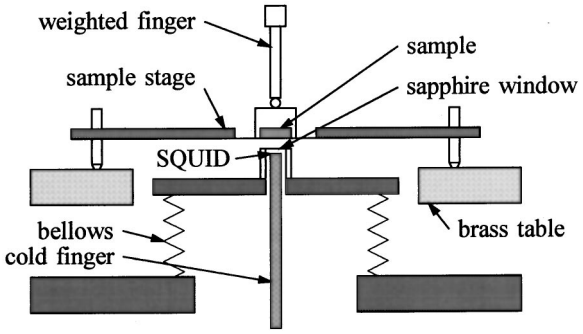

FIG. 3. Schematic of SQUID microscope.

screws rests on a large brass table mounted with a kinematic mount, allowing the sample stage and table to be aligned with the vacuum window. A thin piece of aluminum couples the sample stage to a two-dimensional (2D) translation stage, providing rigidity in the plane of the 2D motion while allowing the stage to tilt and move in the plane perpendicular to the 2D motion. The sample is mounted on a mylar film attached to the sample stage while a weighted finger holds the sample against the vacuum window, maintaining a constant SQUID-to-sample separation. A computer raster scans the sample stage over the SQUID by stepper motors while recording the SQUID signal. Since the SQUID measures the magnetic field component perpendicular to the sample surface, the scanning produces a 2D image of the magnetic field due to the remanent magnetization of the sample.

IV. RESULTS AND DISCUSSION

A. Microstructures

In the Fe–Cr–Ni alloy system, there are two distinct martensitic transformation products: α' phase and ϵ phase. The α' phase is ferromagnetic, while the ϵ phase is paramagnetic like the parent γ phase. Hence, the magnetic etching technique reveals only the ferromagnetic α' phase. Figure 4 shows the typical microstructures of the inhomogeneously heat-treated sample A after the magnetic etching. The microstructures at $y=20$ mm, 25 mm, 30 mm, and 35 mm [Fig. 1(a)] are shown in (a), (b), (c), and (d), respectively. The microstructures in the region y less than 20 mm are not shown, since the ferromagnetic α' phase was completely absent. Except for this region, as shown in Fig. 1(a), the amount of the α' phase gradually increases along y. As a consequence, the sample becomes a magnetic functionally graded material (FGM).

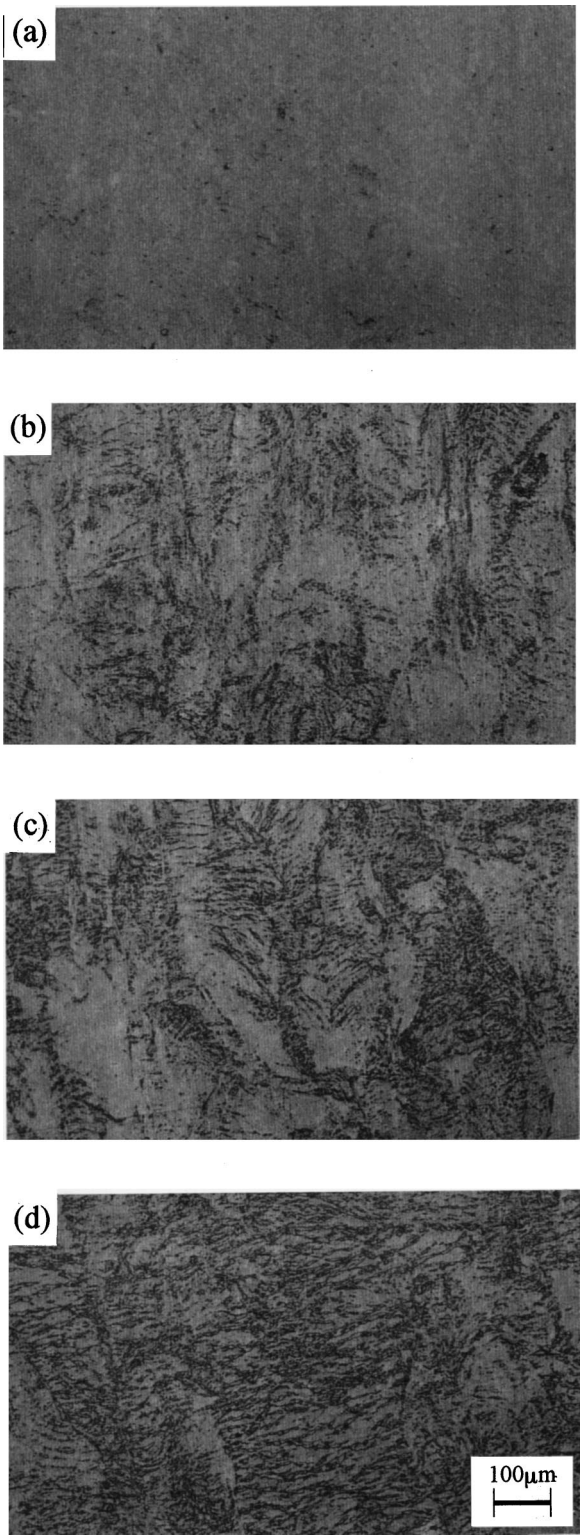

FIG. 4. Distribution of α' martensite in sample A at $y=20$ mm (a), $y=25$ mm (b), $y=30$ mm (c), and $y=35$ mm (d) positions.

B. Hysteresis curves and magnetic properties distributions

Figures 5(a) and 5(b) show the hysteresis curves as a function of the applied magnetic field obtained from the VSM measurements of samples 1 and A, respectively. The detailed profiles of the curves near the origin are also shown in the figure. Note that the magnetization curves depend on the deformation gradient x (sample 1) or the temperature gradient y (sample A). This can be explained by the fact that the amount of the ferromagnetic α' phase varies as a function of x or y, for example, as shown in Fig. 4.

From the hysteresis curves such as that shown in Fig. 5, one can calculate the saturation magnetization, remanent magnetization, and coercive force curves along the samples.

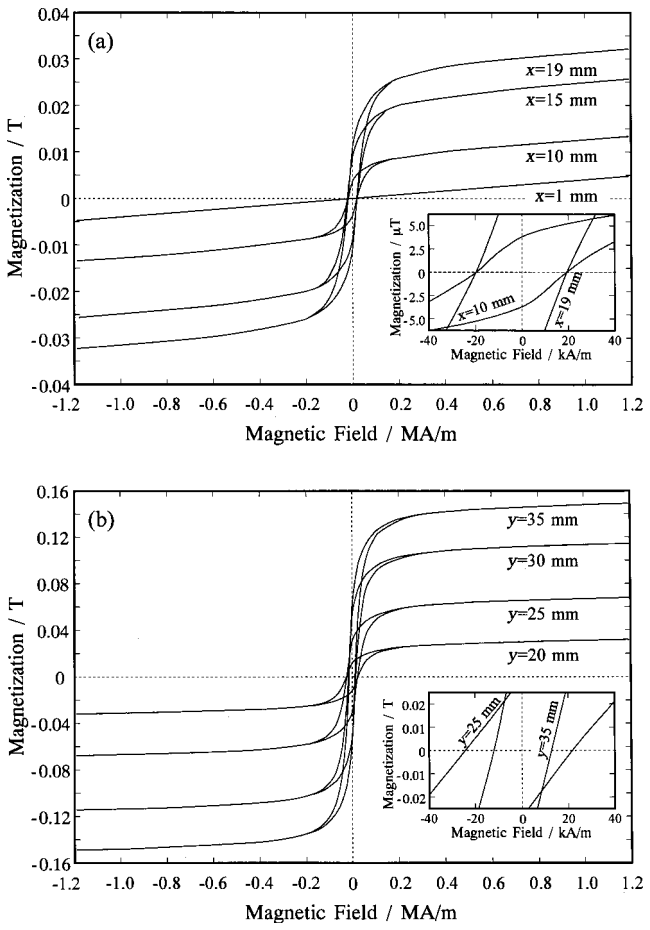

FIG. 5. Hysteresis curves obtained by VSM measurements. (a) sample 1 and (b) sample A.

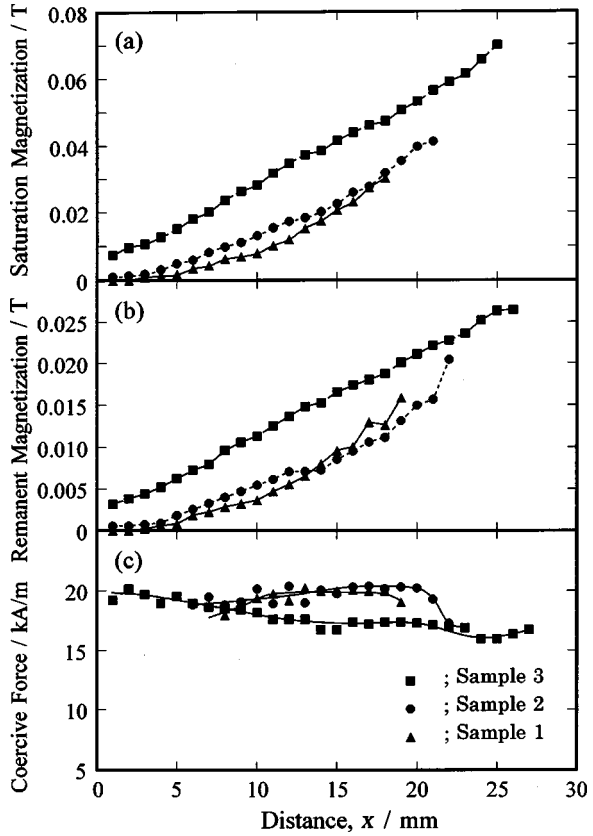

FIG. 6. Saturation magnetization (a), remanent magnetization (b), and coercive force (c) distributions in the rolled samples.

Figure 6 plots these parameters as a function of x for the rolled samples. Note that the difference in these samples is the rolling ratio distribution, i.e., the mechanical deformation gradient over the samples. For samples 1, 2, and 3, the rolling ratios along x range from 0% to 54.6%, from 12.6% to 60.5%, and from 31.3% to 69.9%, respectively. In Fig. 6(a), the saturation magnetization gradually increases as a function of x. This is expected, since the amount of the ferromagnetic α' martensite phase increases with increasing the plastic deformation along the direction. Also, a similar behavior is observed for the remanent magnetization curves. (Since the rolling ratio distributions for samples 1 and 2 are relatively similar, there are only minimal differences in remanent and saturation magnetizations for samples 1 and 2.) Despite the fact that the saturation magnetization and the remanent magnetization gradually increase as a function of x, there was no notable position dependence on the coercive force.

To discuss the above phenomena quantitatively, the remanent magnetization and coercive force in the rolled samples are replotted against the saturation magnetization and are shown in Fig. 7. As can be seen, linear dependence was found between the saturation magnetization and the remanent magnetization, while the coercive force is almost constant with the saturation magnetization. (The coercive force slightly decreases as the saturation magnetization increases.) The magnetization is defined as the magnetic moment per unit volume of a solid. Therefore, the values of saturation magnetization and remanent magnetization are proportioned to the amount of ferromagnetic phase in the sample. On the other hand, however, the coercive force is essentially independent of the amount of ferromagnetic phase. Ding *et al.* studied magnetic properties of martensite–austenite mixtures in mechanically milled 304 stainless steel, and it was found that the coercive force measured at room temperature decreased with the fraction of martensite, due to the increased interaction between the ferromagnetic martensite grains.[11] Therefore, the slight change in the coercive force found in Fig. 7 may occur by the above mechanism.

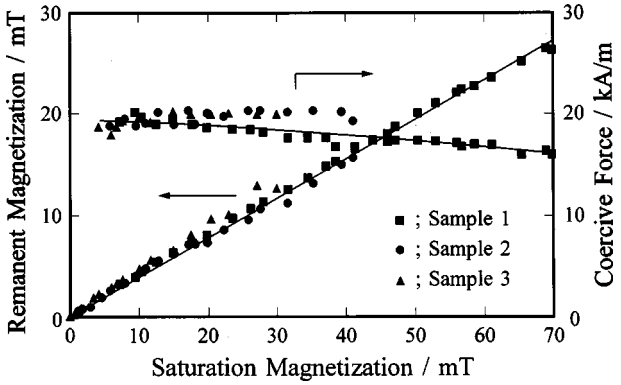

FIG. 7. Remanent magnetization and coercive force in the rolled samples plotted against the saturation magnetization.

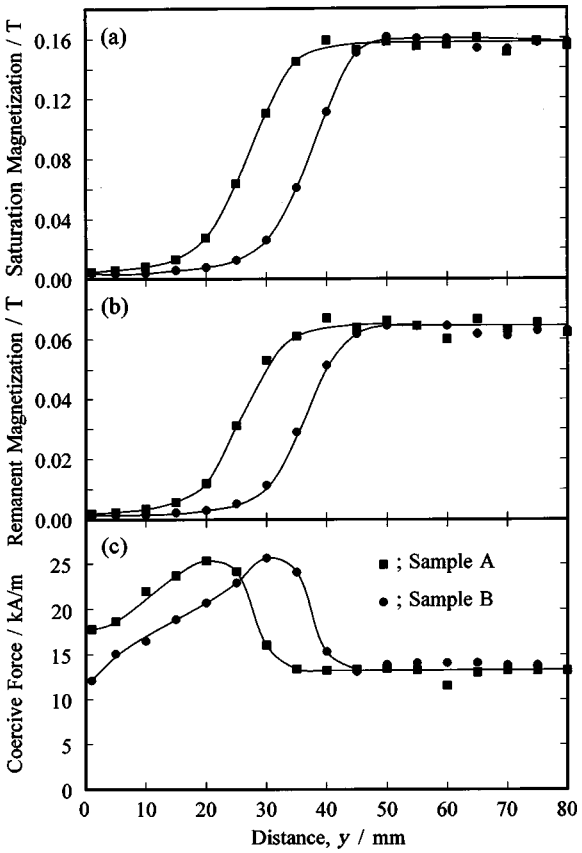

FIG. 8. Saturation magnetization (a), remanent magnetization (b), and coercive force (c) distributions in the heat-treated samples.

In the case of the heat-treated samples (A and B), Fig. 8 plots the saturation magnetization, remanent magnetization, and coercive force curves as a function of y (temperature gradient). Both the saturation magnetization and the remanent magnetization values increase with increasing y. This is due to the fact that the heat treatment promotes larger amounts of the ferromagnetic α' martensite phase along this direction. Furthermore, unlike the behavior shown in Fig. 7(a), the coercive force changes along the sample when y is smaller than 50 mm.

Figure 9 shows the remanent magnetization and coercive force in the heat-treated samples, which are replotted against

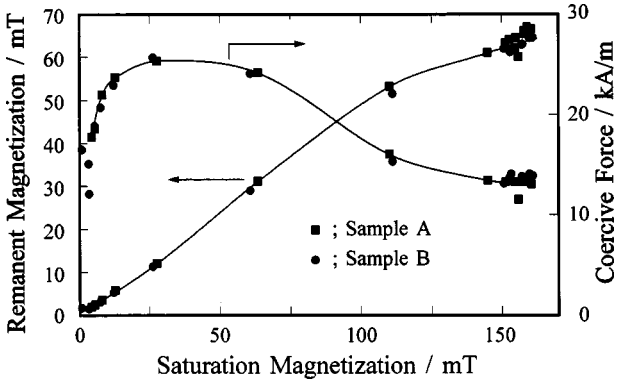

FIG. 9. Remanent magnetization and coercive force in the heat-treated samples plotted against the saturation magnetization.

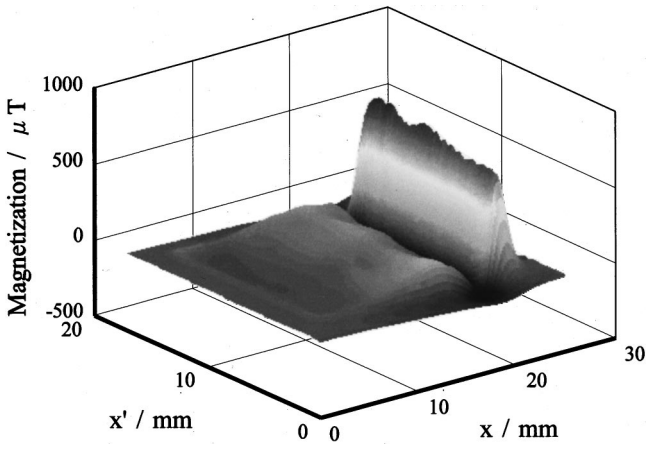

FIG. 10. Magnetic field image from sample 1.

the saturation magnetization. A linear dependence was found between the saturation magnetization and the remanent magnetization similar to the rolled samples. In contrast, the coercive force of the heat-treated sample dramatically changes with the saturation magnetization. This is associated with the fact that the heat treatment of the Fe–Cr–Ni system introduced the carbide and/or nitride precipitates. It is well recognized that these fine precipitates can interact with the domain walls and limit their movement, thereby increasing coercivity.

C. Magnetic field images

Figure 10 shows the magnetic field image of the sample 1 (rolled sample) obtained by the SQUID microscope. Note that the remanent field increases along the deformation gradient, which is in agreement with the results from the optical microscope and VSM measurements presented above. A large peak is observed at one end ($x=12.7$ mm) of the image. In general, the local demagnetization factor is low at the edges and high at the center. Since only the free edge has a substantial martensite content, it will become highly magnetized due to the higher effective field (the applied field—the demagnetizing field) during the magnetization process. It will then have a higher remanent field than a comparable microstructure at the center of the specimen. On the other hand, the opposite edge ($x=0$) has a low martensite and a high austenite content and will not show a high remanent field. The other possibility of the large peak is that the irregular geometry of the free edge produces a large effect on magnetization. At the end of the rolled samples, there is always a concavity in the through-thickness profile. If a thin region is then exposed, the demagnetizing factor is lower and produces a larger magnetization at the region.

The presence of this large magnetization can create an oppositely oriented, compensating field in the neighboring regions, resulting in the double peak seen in Fig. 10. This oppositely oriented field cancels the field due to the deformation gradient near the large edge peak. Away from the edge peak, there is a gradual decrease in the vertical component of the remanent magnetization going down the deformation gradient. This suggests that SQUID microscopy can

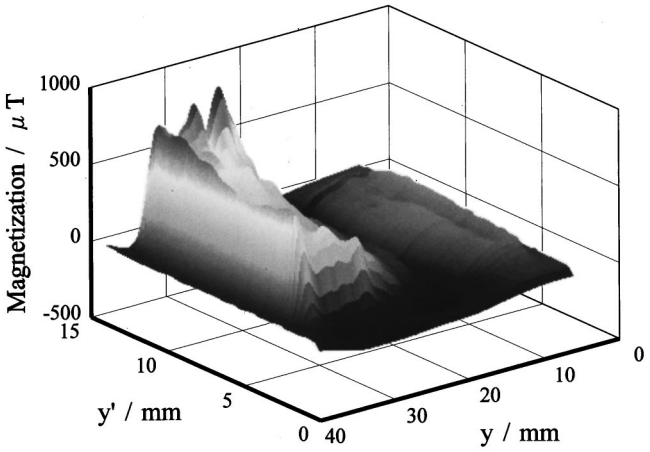

FIG. 11. Magnetic field image from sample A.

become a valuable technique that measures material properties associated with the martensitic transformation. This microscope may have potential applications not only in detecting phase transformation but also in examining the defects structures of the materials.

Figure 11 shows the magnetic field image of sample A (heat-treated sample) obtained by the SQUID microscope. As can be seen, the remanent field decreases along the temperature gradient, which is in agreement with the results from the optical microscope and VSM measurements presented above.

We are currently investigating the relationship between the changes in physical metallurgy of steel due to thermal aging and mechanical stress and the accompanying changes in remanent magnetization. This may lead to the determination of the structural integrity of steel by a simple and nondestructive measurement of its remanent magnetization with the SQUID microscope.

V. SUMMARY

The magnetic FGMs were fabricated by a nonuniform mechanical deformation or an inhomogeneous heat treatment of the Fe–Cr–Ni alloy. The magnetic characteristics were examined by the VSM technique and a SQUID microscope. The SQUID images were in agreement with the results from the VSM measurements and microstructural analysis. This work suggests that a simple SQUID measurement may become an effective method for the NDE of ferromagnetic steels by correlating the remanent magnetization images to the microstructural characteristics.

ACKNOWLEDGMENTS

One of the authors (Y.W.) gratefully acknowledges the financial support from Grant-in-Aid for COE Research (10CE2003) by the Ministry of Education, Science, Sports and Culture of Japan. Work done at LBNL was supported by the Director, Office of Energy Research, Office of Basic Energy Sciences, U. S. Department of Energy, under Contract No. DE-AC03-76SF00098.

[1] J. Clarke, *SQUID Sensors: Fundamentals, Fabrication and Applications*, edited by H. Weinstock (Kluwer Academic, Dordrecht, 1996), pp. 1–62.
[2] T. J. Shaw, K. Schlenga, R. McDermott, J. Clarke, J. W. Chan, S. H. Kang, and J. W. Morris, Jr., IEEE Trans. Appl. Supercond. **9**, 4107 (1999).
[3] P. L. Mangonon, Jr. and G. Thomas, Metall. Trans. **1**, 1587 (1970).
[4] M. A. M. Bourke, J. G. Maldonado, D. Masters, K. Meggers, and H. G. Priesmeyer, Mater. Sci. Eng., A **221**, 1 (1996).
[5] H. Sakai, D. Morishita, and Y. Watanabe, Mater. Sci. Forum **308-311**, 579 (1999).
[6] Y. Watanabe, Y. Nakamura, Y. Fukui, and K. Nakanishi, J. Mater. Sci. Lett. **12**, 326 (1993).
[7] Y. Watanabe, Y. Nakamura, and Y. Fukui, Functionally Graded Materials 1996 (Proceedings of FGM'96), pp. 713–718, 1997.
[8] Y. Watanabe, S. H. Kang, J. W. Chan, and J. W. Morris, Jr., Mater. Trans., JIM **40**, 961 (1999).
[9] Z. Mei and J. W. Morris, Jr., Metall. Trans. A **21A**, 3137 (1990).
[10] T. S. Lee, E. Dantsker, and J. Clarke, Rev. Sci. Instrum. **67**, 4208 (1996).
[11] J. Ding, H. Huang, P. G. McCormick, and R. Street, J. Magn. Magn. Mater. **139**, 109 (1995).